Estimation of spinal loading using inertial motion capture and ground reaction force prediction: A validation study

Frederik G. Larsen[a], Frederik P. Svenningsen[a]

[a] Faculty of Health Science and Technology, Aalborg University

ARTICLE INFO

Master Thesis, 07 June 2018

Keywords:
Musculoskeletal modelling
Spine biomechanics
Ground reaction forces and moments
AnyBody Modelling System
Manual materials handling

ABSTRACT

Three-dimensional analysis of the musculoskeletal system typically involves measurements of ground reaction forces and moments (GRF&Ms) with floor-mounted force plates and segment kinematics measured with optical cameras that are expensive and inconvenient to use in the field. Recent advances in inertial motion capture (IMC) provides new opportunities of full-body motion capture in any working environment. Also, newly developed methods allow the prediction of GRF&Ms with only full-body segment kinematic as input to a musculoskeletal model. In the present study, a novel analysis approach was investigated to estimate the internal loading on the lumbar spine exclusively with input from IMC. Validation of the IMC model was done comparing GRF&Ms and L4-L5 joint reaction forces (JRFs) for 13 subjects during common manual materials handling (MMH) tasks with a standard laboratory model. Pearson's correlation coefficients, relative and root-mean-square error, magnitude and phase error were calculated to compare GRF&Ms and L4-L5 JRFs. The results generally showed best agreement for vertical GRFs, sagittal GRMs, frontal GRMs, L4-L5 axial compression forces, and anteroposterior shear forces. The present study proposed a novel method to investigate spine loading in the field using only IMC and musculoskeletal modelling.

1. Introduction

Low back pain (LBP) is the most frequent work-related musculoskeletal disorder (Andersson, 1999), and has been consistently associated with work tasks involving manual materials handling (MMH) (Cole and Grimshaw, 2003; Dempsey, 1998; Waters et al., 2006). MMH tasks such as lifting, imposes high compression forces on the spine, typically measured at L4-L5 and L5-S1 discs (Anderson et al., 1985; Dempsey, 1998; Wilke et al., 2001), which can result in fractures, degeneration of the lumbar vertebrae, or permanent injury to the intervertebral discs and vertebral endplates (Adams and Hutton, 1983; Brinckmann et al., 1998, 1989; Van Dieën et al., 1999). However, the assessment of spinal loads in vivo are challenging and rarely done due to the invasive methods involved (Wilke et al., 2001). For this reason, several other methods have been implemented in an attempt to estimate these forces, including two-dimensional and three-dimensional biomechanical models (van Dieën et al., 2010). Moreover, the impracticality of direct measurements of the compression forces in the spine have led to the development of anatomically detailed, computer-based musculoskeletal models (Dreischarf et al., 2016).

The internal loadings of the musculoskeletal system can be calculated using either forward dynamics or invers dynamics (Pandy and Andriacchi, 2010). In forward dynamics, the muscle forces are estimated by integrating the equations of motion forward in time using neural excitation. Forward dynamics have been applied to understand the cause and effect of lower extremity muscles during e.g. gait (Barrett et al., 2007), however a major drawback from the method is the computation time. Contrarily, in inverse dynamic analysis (IDA) the Newton Euler equations are solved based on measured kinematics to find joint net moments which can be distributed between muscles according to an optimality criterion (Damsgaard et al., 2006).

Previously, de Zee et al. (2007) designed a generic, detailed musculoskeletal model of the spine with seven rigid segments that can be incorporated in IDA to estimate the internal loading of the spinal column. The validity of the generic spine model have been extensively investigated showing good agreement with in vivo intradiscal pressure measurements in the L4-L5 discs during lifting (de Zee et al., 2007; Rajaee et al., 2015; Rasmussen et al., 2009). The generic model was developed in an open source programming language, and several improvements have been made to the original model, including the implementation of joint properties (disc height, rotation angles and stiffness), long and short segmental muscles, intra-abdominal pressure and lumbar ligaments (Han et al., 2012). These additions have improved the performance of de Zee's model, especially during lifting of heavy objects. More recently, Bassani et al. (2017) validated the model with actual motion capture data which showed good agreement with in vivo data from Wilke et al. (2001).

The quantification of body kinematics and kinetics in the workplace would ideally be performed in situ, since

laboratory experiments typically involve simplifying and constrained movements to some extent, as well as excluding other workplace factors (e.g. physical constraints, workplace culture etc.) (Kim and Nussbaum, 2013). Until recently accurate IDA in the field would involve camera based motion capture and floor-mounted force plates (Faber et al., 2008) or instrumented force shoes (Veltink et al., 2005). However, due to the evolution in methods to predict GRF&Ms, IDA in the field mainly depends on the ability to obtain accurate segment kinematics of the full body (Fluit et al., 2014; Karatsidis et al., 2018; Peng et al., 2017; Skals et al., 2017a, 2017b). Recent advances in ambulatory motion tracking systems, such as inertial motion capture (IMC), allow the application of full-body motion capture in any working environment without the drawback from magnetic distortions (Filippeschi et al., 2017; Roetenberg et al., 2013). Kinematic input to a musculoskeletal model using orientation estimates from full-body ambulatory IMC measurements have already been assessed (Koning et al., 2015), and tested with inverse dynamic calculations (Karatsidis et al., 2018). However, the validity full-body analysis during typical MMH task have yet to be investigated before such analysis approaches are performed in the field.

Therefore, the aim of the present study was to validate the estimation of L4-L5 spinal forces based on a musculoskeletal model driven exclusively using IMC data and ground reaction force prediction during various lifting and transferring tasks. To achieve this, we compared the joint reaction forces (JRFs) at the L4-L5 discs and the predicted GRF&Ms to an optical motion capture and force plate-driven musculoskeletal model. This approach will help determine if musculoskeletal models driven by IMC-data and ground reaction force prediction can be used to estimate spinal loading during MMH tasks in the field.

2. Methods

2.1 Subjects

9 healthy males and 4 healthy females (age 25.7 ± 3.3 years, height 179.3 ± 7.8 m, weight 76.6 ± 12.0 kg) with no present musculoskeletal or neurological disorders participated in the study. The study followed the ethical guidelines from The North Denmark Regional Committee on Health Research Ethics and all subjects provided written informed consent prior to data collection.

2.2 Instrumentation

Motion analysis was performed using the OMC and IMC systems simultaneously. Full-body trajectories of 42 passive reflective markers were recorded with 8 infrared Oqus cameras (Qualisys, Göteborg, Sweden) sampling at 120 Hz. The marker protocol was similar to Karatsidis et al. (2016) and is shown in Appendix 1. Also, full-body kinematics were measured using 17 inertial measurement units (IMUs) (Xsens MVN Awinda, Xsens Technologies BV, Enschede, The Netherlands) sampling at 60 Hz. The placement of the 17 strap-based IMUs is shown in Appendix 1. GRF&Ms (Fx, Fy, Fz, Mx, My, Mz) were measured using three floor-mounted force plates (AMTI, Watertown, MA, USA), one placed beneath each foot and one beneath the box, sampling at 1200 Hz. All measurements were synchronized using a TTL trigger in Xsens MVN Analyze (v.2018.0.0).

2.3 Experimental procedure

The experimental session lasted approximately two hours. Initially, the IMUs and reflective markers were attached to the subjects. As a preventive measure for reducing soft-tissue artefacts (STA) for the reflective markers, the male participants were shirtless and thus not using the provided Xsens MVN Awinda shirt. The shoulder, pelvis, and sternum IMUs were attached with double-sided tape to the skin. Due to variations in anthropometric measurements, several body dimensions were entered manually into the MVN software. Subsequently, subjects were asked to stand in an N-pose and perform a short walking trial to calibrate the IMC system (Cutti et al., 2010; Roetenberg et al., 2013; Xsens Technologies, 2017).

All subjects performed six different lifting tasks and two transferring tasks in their own pace, including symmetrical lifting, asymmetrical lifting, and load transferring, as illustrated in Fig. 1. Specifically, the lifting tasks (LIFTUP-5/10) involved lifting a box (0.40 x 0.295 x 0.235 m) of different weights (5, 10 kg) from the ground to an upright position and back to the starting point. Load transferring (TRA-5/10) involved moving a box of different weights (5, 10 kg) from a table of 1 m height to a similar table and back to the starting point. The tables were placed to the right and left of the participant at 0.2 m distance from the right and left foot. The symmetric (SYM-5/10) and asymmetric lifting (ASYM-5/10) tasks involved lifting a box with different weights (5, 10 kg) from the floor and place it on a table at 0.8 m height for both tasks. For ASYM-5/10 conditions, the table was placed to the right of the participant at 0.2 m distance from the right foot, whereas for SYM-5/10 conditions, the table was placed in front of the participant. Prior to data collection, the participants performed all tasks to familiarize them to the movements. Three repetitions were performed for each task in a randomized order totaling 24 lifts for each subject.

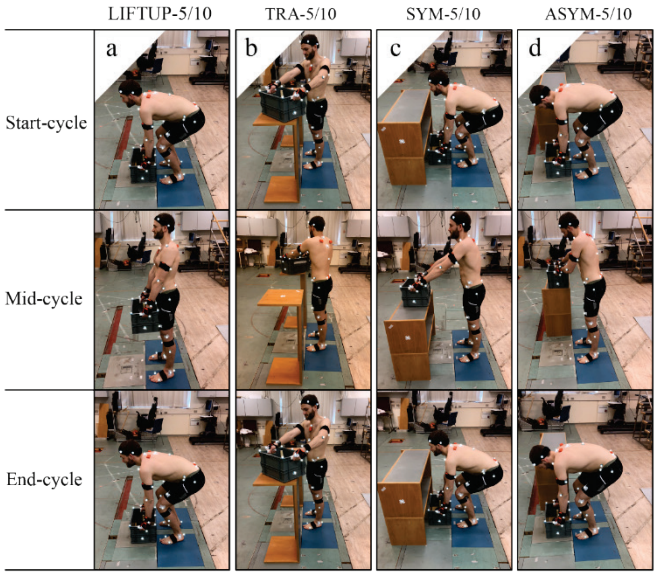

Fig. 1: a-d: Lifting and transferring phases from start-cycle to mid-cycle to end-cycle. LIFTUP-5/10 (a) includes lifting a 5-10 kg box to an upright position. TRA-5/10 (b) includes transferring of a 5-10 kg box between two tables. SYM-5/10 (c) includes symmetric lifting and placing of a 5-10 kg box on a table. ASYM-5/10 (d) includes asymmetric lifting and placing of a 5-10 kg box on a table.

2.4 Model setup

The motion data from IMC was exported as a Biovison Hierarchy (BVH) file from the MVN software. The motion data and analog data from OMC was exported as a Coordinate 3D (C3D) file from Qualisys Track Manager 2.16. The 3D coordinate and analog data from OMC and raw 3D coordinate data from IMC was segmented in MATLAB® (R2018a, Mathworks Inc., Natick, MA USA) using the vertical GRF beneath the load, to isolate the period in which the participant was in contact with the load. Concerning the tasks involving transfer, the first and last peak flexion angles from the left shoulder joint were detected from the Xsens IMU data (.mvnx), and the period in between were used to define the period of load contact. From the laboratory measurements, three musculoskeletal models were developed, each driven from a different kinematic and kinetic input: (1) optical motion capture and measured ground reaction forces (OMC-MGRF), (2) optical motion capture and predicted ground reaction forces (OMC-PGRF), and (3) inertial motion capture and predicted ground reaction forces (IMC-PGRF), as illustrated in Fig. 2. The musculoskeletal models were developed in the AnyBody Modelling System (AMS) v. 7.1 (AnyBody Technology, Aalborg, Denmark) using the Plug-in-gait-MultiTrial_StandingRef as template for OMC-MGRF and OMC-PGRF models, while BVH_Xsens was used as the template for the IMC-PGRF model. All templates were extracted from Anybody Managed Model Repository v. 2.1 (Damsgaard et al., 2006). The box used in the experiment were geometrically modelled as a rectangular box in SOLIDWORKS 2017 (Dassault Systèmes S.A., Vélizy-Villacoublay, France) with equivalent dimensions (0.40 x 0.295 x 0.235 m). The inertial properties were computed for each weight (5, 10 kg) around the center of the object. Additional programming code in AMS generated the box in the model with information about mass, orientation, location, size, inertia, and rigid connections between the box to the hands.

OMC-MGRF was considered the golden standard, as it is the most commonly used system for providing kinematic and kinetic input to musculoskeletal models. The models had 39 degrees of freedom and the lower extremity model was based on the cadaver study of Carbone et al. (2015), the lumbar spine model was based on the work of de Zee et al. (2007), Hansen et al. (2006), and the enhancements of Han et al. (2012), and the shoulder and arm models were based on the research from Van Der Helm et al. (1992) and Veeger et al. (1997, 1991). The spine model was actuated by 188 muscle elements, modeled with non-linear disc stiffness in the lumbar region, and with ligaments and an intra-abdominal pressure applied similar to Han et al. (2012). All segments were modeled as rigid-bodies, and the spine model consisted of seven rigid segments describing the cervical, thorax, and lumbar vertebras as well as the sacrum (de Zee et al., 2007; Hansen et al., 2006). The model followed a spine rhythm that distributes the trunk motion over the vertebral bodies using a coupled-mechanism (Hansen et al., 2006; Wong et al., 2006).

2.5 Model scaling

For each subject, a musculoskeletal model was created using a single symmetric lifting trial based on the OMC data. The anthropometry of the OMC models were scaled based on the position of the reflective markers according to Andersen et al. (2009; 2010). Data obtained using IMC were imported into AMS together with the BVH_Xsens musculoskeletal model. The BVH_Xsens model automatically scaled the segment lengths according to the joint-to-joint distances of the stick figure contained in the .bvh files. Additional nodes were added to the musculoskeletal model to unscaled segments (pelvis, foot, and trunk) equivalent to points on the stick figure.

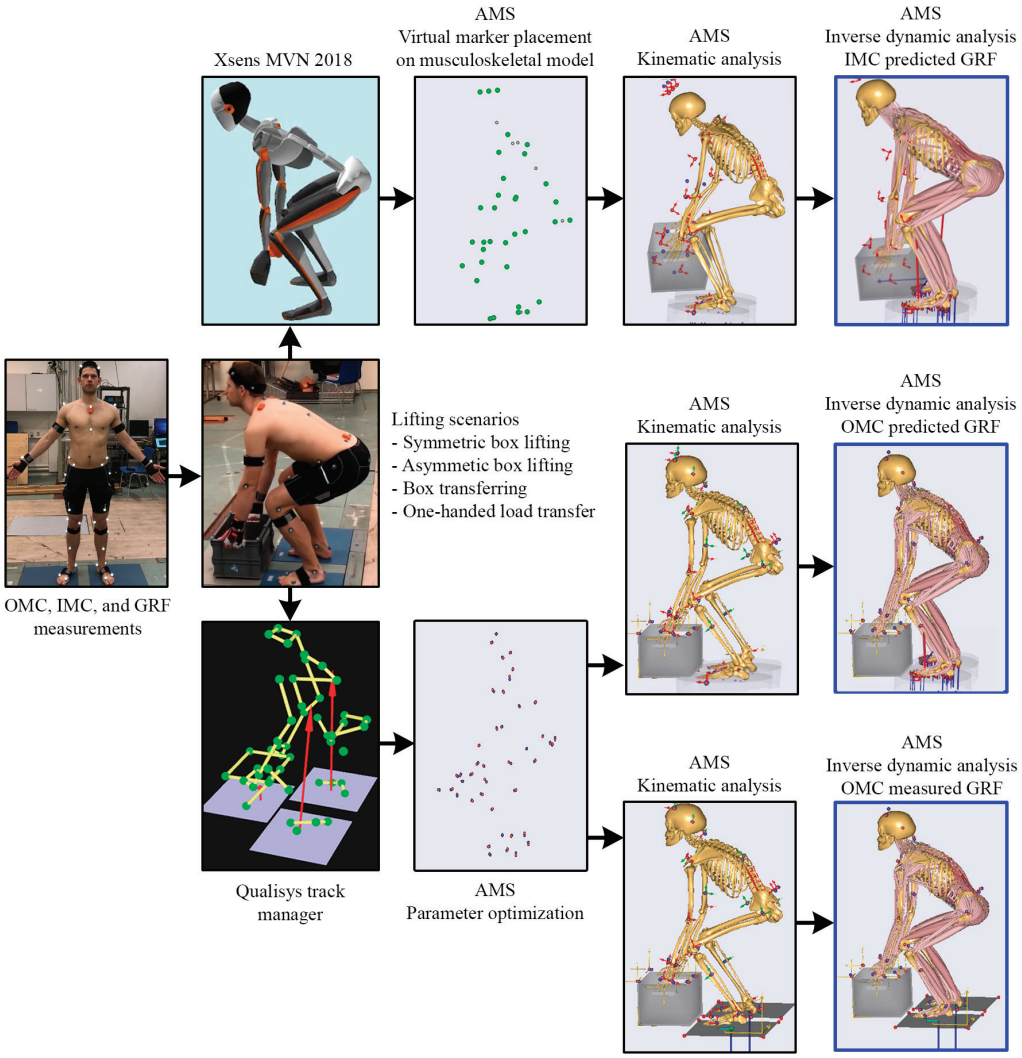

Fig. 2: Flowchart of the process for developing the three models: 1) IMC-PGRF, 2) OMC-PGRF, and 3) OMC-MGRF.

The ratio between the unscaled segments and the distance between the added nodes were multiplied onto the segment lengths on the stick figure before applying it to the BVH_Xsens model. Virtual markers were introduced on both the stick figure and the musculoskeletal model to perform marker tracking between the two models. A nonlinear least-square optimization problem which minimize the least-square difference of the virtual markers between the two models, was applied to ensure optimally tracking (Andersen et al., 2009). Further details can be found in Skals et al. (2017b) and Karatsidis et al. (2018). Lastly, the anthropometry of the IMC models were scaled according to constructed virtual markers (Andersen et al., 2010, 2009), and the body mass was linearly distributed to the segments according to the regression equations of Winter (2009). The development of the three musculoskeletal models is illustrated in Fig. 2. The reflective and inertial marker trajectories and force measurements were digitally filtered using a second order Butterworth filter with a cut-off frequency set to 6 Hz for marker trajectories and 15 Hz for force measurements.

2.6 Muscle recruitment

Muscle recruitment was solved by formulating an optimization problem that distributes the muscle forces according to an optimality criterion, where the goal is to minimize the largest relative load of any muscle in the musculoskeletal system (Damsgaard et al., 2006; Rasmussen et al., 2001):

$$\underset{f}{minimize} \quad G\left(f^{(M)}\right) = \sum_{i=1}^{n^{(M)}} \left(\frac{f_i^{(M)}}{N_i}\right)^3 \tag{1a}$$

$$subject\ to \quad \boldsymbol{Cf} = \boldsymbol{d} \tag{1b}$$

$$0 \le f_i^{(M)}, i = 1, \dots, n^{(M)} \tag{1c}$$

where G is the third order polynomial objective cost function, $f_i^{(M)}$ the muscle force of the ith muscle, $n^{(M)}$ the number of muscles, and N_i the strength of the muscle. $\boldsymbol{C}$ is the coefficient matrix for the dynamic equilibrium equations, $\boldsymbol{f}$ is all the unknown muscle and joint reaction forces, and $\boldsymbol{d}$ contains all the external and inertial forces. Furthermore, the non-negativity constraint dictates that the muscles can only pull. Muscles were modeled as simple muscles without contraction dynamics, and their strength depended only on the physiological cross-sectional area. The strength of each muscle was determined from a mass-fat scaling law (Frankenfield et al., 2001; Rasmussen et al., 2005).

2.7 Prediction of ground reaction forces and moments

GRF&Ms were predicted for IMC-PGRF and OMC-PGRF models. The method was similar to that of previous studies (Fluit et al., 2014; Karatsidis et al., 2018; Peng et al., 2017; Skals et al., 2017a, 2017b). 25 dynamic contact elements were attached under each foot. The contact elements consisted of five uniaxial force actuators that can generate positive vertical, anteroposterior, and mediolateral static friction forces that balance the equilibrium equations in (1b). Furthermore, a non-linear strength function similar to Skals et al. (2017a) was implemented, to accommodate to the fact that contact elements only would generate forces when the elements were close to the ground and stationary. The strength function ensured that the generation of forces only would be activated when the contact points were almost without motion and overlapped with a user-defined artificial ground plane. In order to prevent discontinuities in predicted GRF&Ms due to sudden transitions of contact points from inactive to fully active, a smoothing function were implemented to build up the strength of the actuators gradually until threshold values were reached (Skals et al., 2017a). Lastly, to improve numerical stability, small residual forces were attached to the pelvis with a strength of 10 N and 10 Nm.

2.8 Data analysis

The following variables were extracted from the IDA for all musculoskeletal models: 1) JRFs at the L4-L5 discs including axial compression forces, mediolateral shear forces, and anteroposterior shear forces, 2) GRFs for the right foot, including vertical GRFs, mediolateral GRFs, and anteroposterior GRFs, and 3) GRMs for the right foot, including transverse GRMs, sagittal GRMs, and frontal GRMs which were recalculated in the ankle joint coordinate system. Forces were normalized to percentage body weight (%BW) and moments were normalized to percentage body weight multiplied with body height (%BW·BH) (Moisio et al., 2003). Trials were averaged within each participant for each lifting and transferring task. Individual data series were time-normalized to 200 data points, representing the cycle where the load has no contact with the ground floor (100%).

To assess the agreement between OMC-MGRF, OMC-PGRF, and IMC-PGRF, several comparisons were performed. The absolute and relative agreement for all times series curves were performed using root mean square error (RMSE) and relative root mean square error (rRMSE), similar to Ren et al. (2008). Furthermore, the phase and magnitude percentage error were calculated to estimate the difference in phase and magnitude between the curves (Schwer, 2007; Sprague and Geers, 2003). The Pearson's correlation coefficient, ρ, was also calculated and categorized as weak, moderate, strong and excellent for $\rho \le 0.35$, $0.35 \le \rho \le 0.67$, $0.67 \le \rho \le 0.9$, $0.9 < \rho$, respectively (Taylor, 1990).

3. Results

Tables 1-6 list the results for the GRFs (Table 1-2), GRMs (Table 3-4), and L4-L5 JRFs (Table 5-6) of each of the three models, specifically IMC-PGRF model versus the OMC-MGRF model (Table 1,3,5) and the OMC-PGRF model versus the OMC-MGRF model (Table 2,4,6). Similarly, Fig. 3-5 illustrates time-series curves of the three model estimates of GRFs for the right foot (Fig. 3), GRMs for the right foot (Fig. 4), and L4-L5 JRFs (Fig. 5) across all lifting and transferring cycles performed by the 13 subjects.

Overall, the comparison of IMC-PGRF versus OMC-MGRF models showed lower accuracy in the prediction of GRFs, GRMs, and JRFs for all lifting and transferring tasks in all directions compared to the OMC-PGRF versus OMC-MGRF model. However, strong to excellent Pearson's correlation coefficients were found for vertical GRFs, axial compression forces, and anteroposterior shear forces when comparing the IMC-PGRF versus OMC-PGRF models, whereas mediolateral GRFs showed weak correlations. Phase and magnitude differences were generally small for axial and anteroposterior JRFs, and for vertical GRFs between IMC-PGRF versus OMC-MGRF and OMC-PGRF versus OMC-MGRF models. Also, when comparing these models, GRMs showed generally large discrepancies in all directions.

3.1 Estimated ground reaction forces

Vertical GRFs showed strong to excellent correlations (see Table 1) between IMC-PGRF versus OMC-MGRF for all lifting and transferring tasks (ρ ranging from 0.70 to 0.97), whereas OMC-PGRF versus OMC-MGRF (see Table 2) showed higher correlations, specifically for LIFTUP-5/10 and SYM-5/10, and equally or slightly higher correlations for other tasks (ρ ranging from 0.86 to 0.98). In addition, vertical GRF RMSE values were considerably higher for LIFTUP-10 (RMSE IMC-PGRF: 14.78 % versus OMC-PGRF: 2.44 %) and SYM-10 (RMSE IMC-PGRF: 16.51 % versus OMC-PGRF: 5.16 %). Likewise, rRMSE values showed similar tendency for LIFTUP-10 (rRMSE IMC-PGRF: 35.64 % versus OMC-PGRF: 7.09 %) and SYM-10 (RMSE IMC-PGRF: 40.26 % versus OMC-PGRF: 17.61 %). Magnitude differences were specifically large for IMC-PGRF during tasks involving lifting or transferring of the 10 kg box (M ranging from IMC-PGRF: 12.77 to 25.86 % versus OMC-PGRF: -0.05 to 4.08 %), whereas same tasks with 5 kg showed lower difference (M ranging from IMC-PGRF: -3.83 to 1.03 % versus OMC-PGRF: -0.21 to 2.52 %). Vertical GRF phase differences were small between the two conditions (P ranging from IMC-PGRF: 2.27 to 4.87 % versus OMC-PGRF: 1.08 to 4.33 %). Mediolateral and anteroposterior GRFs generally showed fewer similarities between IMC-PGRF and OMC-MGRF. IMC-PGRF correlations varied between weak to moderate for all tasks except TRA-10 showing strong correlation in both directions, although on the verge to be considered moderate (ρ ranging from 0.11 to 0.68). However, also OMC-PGRF versus OMC-MGRF displayed similar tendency of low similarity as IMC-PGRF, although with stronger correlations (ρ ranging from 0.18 to 0.82). RMSE (ranging from IMC-PGRF: 1.40 to 17.61 % versus OMC-PGRF: 1.05 to 5.70 %) and rRMSE (IMC-PGRF: 17.69 to 90.28 % versus OMC-PGRF: 17.27 to 69.48 %), and phase (IMC-PGRF: 17.83 to 27.02 % versus OMC-PGRF: 19.68 to 23.52 %) demonstrated that both models performed with low accuracy in mediolateral and anteroposterior GRF estimation, compared to OMC-MGRF.

Table 1: IMC-PGRF-based GRFs versus OMC-MGRF for the eight lifting scenarios. ρ = Pearson's correlation coefficient, RMSE = root mean square error (%BW), rRMSE = relative root mean square error (%), M = curve magnitude difference (%), and P = phase difference (%). Results are for vertical GRF, mediolateral GRF, and anteroposterior GRF. All results are presented as mean (± SD).

Activity	Vertical GRF					Mediolateral GRF					Anteroposterior GRF				
	ρ	RMSE	rRMSE	M	P	ρ	RMSE	rRMSE	M	P	ρ	RMSE	rRMSE	M	P
LIFTUP-5	0.87	6.83	21.12	-3.83	2.55	0.26	1.84	30.24	67.92	27.02	0.11	6.15	90.28	-26.67	21.39
		(3.82)	(11.12)	(9.14)	(1.48)		(0.85)	(13.48)	(65.58)	(4.25)		(3.10)	(50.26)	(45.91)	(5.28)
LIFTUP-10	0.89	14.78	35.64	22.52	2.27	0.37	2.91	26.46	155.79	24.16	0.20	6.13	85.59	-33.73	22.83
		(7.82)	(16.69)	(11.11)	(0.83)		(1.90)	(6.26)	(160.2)	(4.38)		(2.84)	(37.75)	(39.84)	(3.80)
TRA-5	0.97	10.66	11.66	1.03	3.87	0.53	2.26	24.83	68.23	22.98	0.40	5.23	77.17	-25.70	19.53
		(2.73)	(2.62)	(8.73)	(0.85)		(2.19)	(8.36)	(73.8)	(6.26)		(3.44)	(35.59)	(62.48)	(6.46)
TRA-10	0.96	17.61	16.40	14.25	4.87	0.67	2.72	17.69	119.67	22.40	0.68	5.17	43.25	-14.95	23.42
		(5.40)	(4.67)	(5.35)	(1.43)		(2.12)	(3.24)	(108.2)	(5.03)		(3.36)	(13.96)	(45.39)	(6.44)
SYM-5	0.82	6.10	18.58	-1.79	2.53	0.58	1.40	23.82	-12.06	22.00	0.56	4.46	59.81	-28.22	17.83
		(3.08)	(7.36)	(8.15)	(1.00)		(0.60)	(4.48)	(21.02)	(2.97)		(2.87)	(35.56)	(30.82)	(8.34)
SYM-10	0.70	16.51	40.26	25.86	3.21	0.47	2.63	21.65	69.27	24.14	0.50	4.83	55.78	-24.45	19.54
		(8.87)	(18.29)	(16.63)	(1.49)		(1.10)	(6.28)	(54.11)	(3.21)		(2.98)	(30.71)	(33.21)	(7.11)
ASYM-5	0.96	7.90	10.39	-1.43	2.61	0.31	2.10	25.85	58.57	26.04	0.29	4.53	50.38	-25.14	21.07
		(2.11)	(2.24)	(5.94)	(0.87)		(0.94)	(7.49)	(42.51)	(3.67)		(2.82)	(21.84)	(34.99)	(5.97)
ASYM-10	0.94	14.97	19.80	12.77	3.59	0.54	2.42	20.73	87.11	19.82	0.20	5.37	61.00	-35.07	23.06
		(5.25)	(6.63)	(4.11)	(0.53)		(0.90)	(7.14)	(24.08)	(2.91)		(2.52)	(15.87)	(31.15)	(2.27)

Table 2: OMC-PGRF-based GRFs versus OMC-MGRF for the eight lifting scenarios. ρ = Pearson's correlation coefficient, RMSE = root mean square error (%BW), rRMSE = relative root mean square error (%), M = curve magnitude difference (%), and P = phase difference (%). Results are for vertical GRF, mediolateral GRF, and anteroposterior GRF. All results are presented as mean (± SD).

Activity	Vertical GRF					Mediolateral GRF					Anteroposterior GRF				
	ρ	RMSE	rRMSE	M	P	ρ	RMSE	rRMSE	M	P	ρ	RMSE	rRMSE	M	P
LIFTUP-5	0.98	2.18	6.91	-0.21	1.08	0.68	1.05	23.03	5.26	22.69	0.45	5.03	63.10	-16.10	20.63
		(0.71)	(2.04)	(1.58)	(0.27)		(0.46)	(7.56)	(25.42)	(4.99)		(2.18)	(41.88)	(54.64)	(7.31)
LIFTUP-10	0.98	2.44	7.09	-0.05	1.14	0.66	1.33	24.88	14.20	23.52	0.36	5.75	69.48	-16.30	22.20
		(0.90)	(2.58)	(2.09)	(0.26)		(0.48)	(9.00)	(26.95)	(5.32)		(2.25)	(49.51)	(47.55)	(5.67)
TRA-5	0.98	8.24	9.07	0.87	3.38	0.81	1.29	25.31	5.44	22.19	0.82	3.68	61.97	-54.94	20.74
		(2.29)	(1.82)	(4.08)	(0.74)		(0.60)	(10.57)	(31.54)	(5.67)		(1.61)	(22.46)	(16.64)	(5.75)
TRA-10	0.96	12.06	10.71	4.08	4.33	0.80	1.32	17.27	19.10	19.68	0.82	3.91	50.84	-46.63	23.14
		(5.08)	(2.45)	(4.49)	(0.89)		(0.38)	(3.95)	(20.19)	(3.48)		(1.51)	(14.60)	(10.34)	(5.99)
SYM-5	0.89	3.58	12.87	2.52	1.74	0.73	1.36	19.06	8.95	20.28	0.61	4.11	49.75	-35.79	20.31
		(1.21)	(6.18)	(1.42)	(0.39)		(0.41)	(6.95)	(29.85)	(5.40)		(1.83)	(26.52)	(17.89)	(6.77)
SYM-10	0.86	5.16	17.61	3.27	2.41	0.67	1.69	19.67	21.20	20.91	0.59	5.18	49.19	-19.86	22.39
		(1.95)	(8.45)	(2.34)	(0.60)		(0.48)	(5.06)	(35.48)	(3.55)		(2.27)	(24.71)	(29.34)	(8.09)
ASYM-5	0.97	6.06	8.22	1.19	2.33	0.59	1.42	23.37	11.63	23.50	0.39	4.54	61.63	-31.80	22.30
		(2.51)	(2.88)	(2.01)	(0.89)		(0.70)	(6.12)	(55.28)	(4.30)		(2.13)	(41.27)	(32.27)	(4.73)
ASYM-10	0.94	9.18	10.95	3.53	3.14	0.72	1.27	18.74	-1.68	21.02	0.18	5.70	60.10	-24.48	22.98
		(3.57)	(3.04)	(1.97)	(0.78)		(0.41)	(4.53)	(13.87)	(3.47)		(2.15)	(22.14)	(36.25)	(5.62)

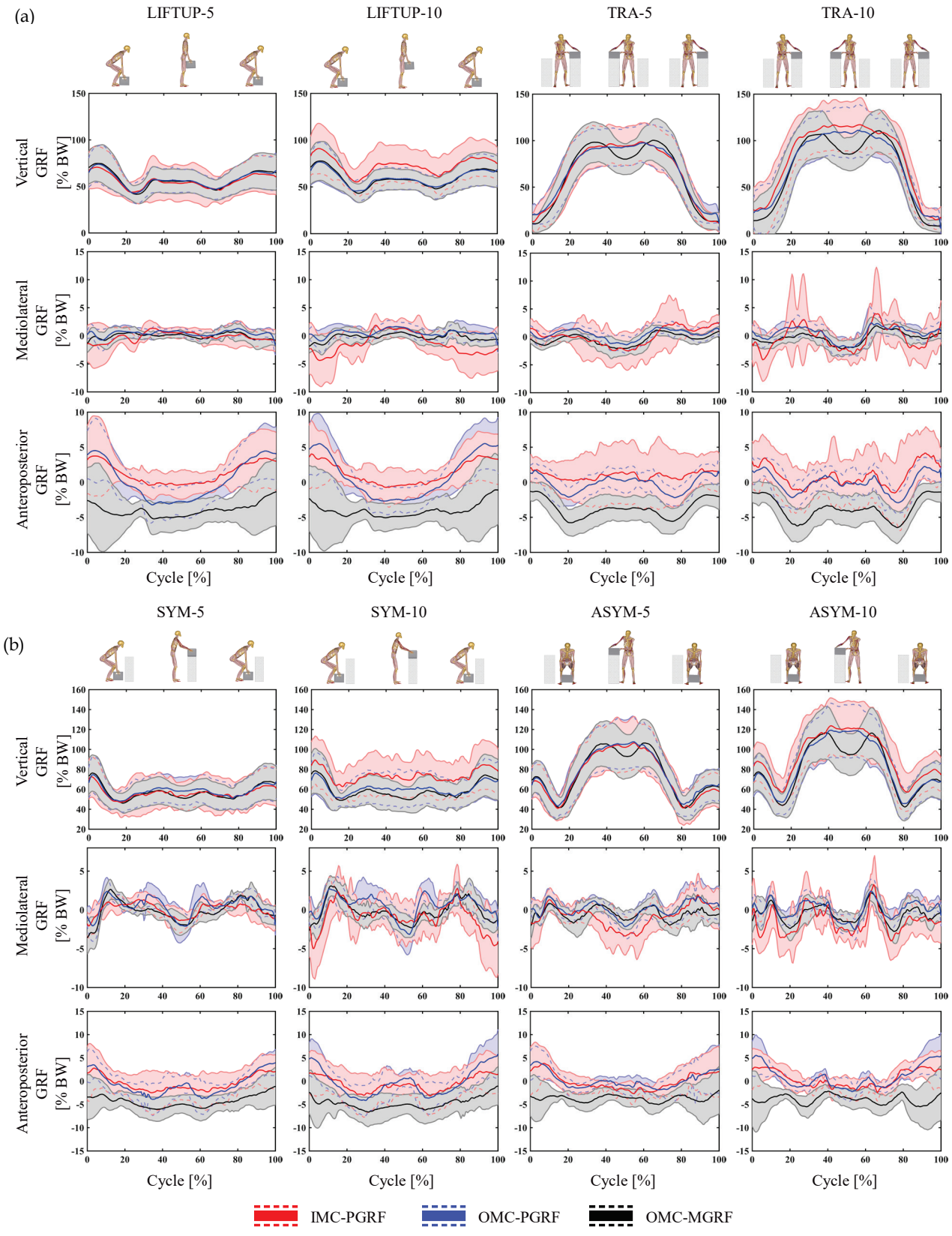

Fig. 3: GRF estimates for the right foot (SD around mean) of the IMC-PGRF (red-shaded area around red line), OMC-PGRF (blue-shaded area around blue line), and OMC-MGRF (black-shaded area around black line) models, illustrating the vertical GRF, mediolateral GRF, and anteroposterior GRF from (a) LIFTUP-5, LIFTUP-10, TRA-5, TRA-10, and (b) SYM-5, SYM-10, ASYM-5, and ASYM-10.

3.2 Estimated ground reaction moments

GRMs showed generally large discrepancies when comparing IMC-PGRF versus OMC-MGRF (see Table 3). The symmetrical lifting tasks LIFTUP-5/10 and SYM-5/10 all had weak correlations for transverse GRMs (ρ ranging from -0.12 to -0.05 %), whereas ASYM-5/10 showed moderate correlations (ρ: 0.27 and 0.46). TRA-5/10 tasks displayed a correlation of in transverse (ρ: 0.70 and 0.79) and in sagittal (ρ: 0.85 and 0.84) GRMs. Similar results were observed for OMC-PGRF versus OMC-MGRF (see Table 4), showing strong correlations for transfer tasks and asymmetric lifting tasks and weak to moderate correlations for the symmetrical lifting tasks. Frontal GRMs seemed to correlate with higher accuracy for both models versus OMC-MGRF (ρ ranging from IMC-PGRF: 0.48 to 0.80 versus OMC-PGRF: 0.53 to 0.90). Transverse GRM rRMSE values tended to be lower for IMC-PGRF than for OMC-PGRF (rRMSE ranging from IMC-PGRF: 26.02 to 67.75 % versus OMC-PGRF: 48.86 to 87.04 %), whereas both sagittal and frontal GRMs showed higher rRMSE values for IMC-PGRF. However, both models seem to exhibit large discrepancies to OMC-MGRF for all tasks in all directions (rRMSE minimum value for IMC-PGRF: 21.83 % and OMC-PGRF: 16.21 %). Also, large inter-subject magnitude variabilities were observed in all directions, displaying that both IMC-PGRF and OMC-PGRF models were over- and underestimating GRMs. In addition, phase differences were consistent in all directions, specifically for transverse GRMs (P ranging from IMC-PGRF: 13.88 to 25.89 % and OMC-PGRF: 20.35 to 26.67 %), although not as prominent as magnitude differences.

Table 3: IMC-PGRF-based GRMs versus OMC-MGRF for the eight lifting scenarios. ρ = Pearson's correlation coefficient, RMSE = root mean square error (%BW), rRMSE = relative root mean square error (%), M = curve magnitude difference (%), and P = phase difference (%). Results are for transverse GRM, sagittal GRM, and frontal GRM. All results are presented as mean (± SD).

Activity	Transverse GRM					Sagittal GRM					Frontal GRM				
	ρ	RMSE	rRMSE	M	P	ρ	RMSE	rRMSE	M	P	ρ	RMSE	rRMSE	M	P
LIFTUP-5	-0.05	0.01	67.75	43.30	24.47	0.38	0.01	53.41	8.92	11.25	0.76	0.01	41.83	-19.52	10.23
		(0.004)	(19.80)	(91.15)	(9.02)		(0.003)	(26.74)	(100.81)	(4.00)		(0.01)	(28.42)	(39.50)	(4.39)
LIFTUP-10	-0.11	0.01	53.85	19.81	25.05	0.67	0.01	37.67	73.84	8.10	0.80	0.01	29.61	-17.92	8.82
		(0.004)	(16.34)	(60.56)	(6.44)		(0.01)	(18.22)	(76.81)	(3.80)		(0.01)	(19.02)	(27.08)	(3.78)
TRA-5	0.70	0.01	56.07	-32.99	13.88	0.85	0.01	37.73	58.79	11.68	0.71	0.01	40.30	-8.79	10.90
		(0.005)	(45.84)	(30.33)	(7.12)		(0.01)	(30.53)	(91.99)	(7.06)		(0.005)	(41.99)	(26.17)	(2.36)
TRA-10	0.79	0.01	26.02	51.65	14.72	0.84	0.02	38.36	133.09	10.38	0.57	0.02	34.84	12.12	13.65
		(0.004)	(27.27)	(51.62)	(4.15)		(0.01)	(12.10)	(100.1)	(6.03)		(0.01)	(11.76)	(27.20)	(2.60)
SYM-5	-0.09	0.01	45.28	13.14	25.89	0.53	0.01	39.03	39.60	11.86	0.73	0.01	21.83	-0.01	12.22
		(0.003)	(13.52)	(37.96)	(5.65)		(0.004)	(14.20)	(59.5)	(4.48)		(0.003)	(7.03)	(25.03)	(3.47)
SYM-10	-0.12	0.01	40.08	7.61	23.57	0.55	0.01	47.26	110.07	9.77	0.48	0.02	29.71	29.72	13.22
		(0.003)	(17.73)	(34.69)	(4.46)		(0.01)	(18.81)	(126.1)	(2.52)		(0.01)	(10.68)	(37.61)	(5.16)
ASYM-5	0.27	0.01	33.94	30.18	21.84	0.81	0.01	23.73	52.08	11.22	0.77	0.02	27.26	-21.03	11.81
		(0.003)	(7.39)	(50.15)	(7.23)		(0.01)	(6.85)	(66.87)	(2.33)		(0.01)	(9.90)	(16.66)	(2.82)
ASYM-10	0.46	0.01	27.72	54.55	19.01	0.80	0.02	31.79	101.81	9.94	0.68	0.02	23.13	6.18	11.14
		(0.003)	(11.65)	(47.00)	(4.52)		(0.01)	(8.31)	(72.23)	(2.51)		(0.01)	(5.69)	(17.24)	(1.83)

Table 4: OMC-PGRF-based GRMs versus OMC-MGRF for the eight lifting scenarios. ρ = Pearson's correlation coefficient, RMSE = root mean square error (%BW), rRMSE = relative root mean square error (%), M = curve magnitude difference (%), and P = phase difference (%). Results are for transverse GRM, sagittal GRM, and frontal GRM. All results are presented as mean (± SD).

Activity	Transverse GRM					Sagittal GRM					Frontal GRM				
	ρ	RMSE	rRMSE	M	P	ρ	RMSE	rRMSE	M	P	ρ	RMSE	rRMSE	M	P
LIFTUP-5	-0.11	0.01	76.65	58.01	24.18	0.29	0.004	43.00	6.23	11.03	0.90	0.004	16.47	-4.42	5.34
		(0.005)	(26.36)	(90.13)	(7.06)		(0.002)	(19.40)	(22.22)	(6.49)		(0.002)	(5.03)	(9.36)	(1.77)
LIFTUP-10	-0.07	0.01	78.28	46.27	23.65	0.32	0.004	37.28	17.84	9.90	0.89	0.01	16.59	-4.57	5.06
		(0.01)	(18.71)	(65.11)	(5.67)		(0.001)	(15.90)	(25.26)	(5.62)		(0.001)	(6.36)	(9.85)	(1.18)
TRA-5	0.90	0.01	87.04	-65.00	26.30	0.89	0.01	21.03	42.05	7.56	0.75	0.01	26.13	-2.06	10.28
		(0.002)	(40.33)	(9.82)	(6.12)		(0.003)	(6.27)	(27.42)	(2.79)		(0.003)	(5.07)	(18.06)	(2.67)
TRA-10	0.89	0.01	54.57	-55.12	20.35	0.85	0.01	25.82	62.72	9.68	0.70	0.02	22.31	12.94	12.44
		(0.002)	(19.05)	(14.13)	(5.99)		(0.004)	(6.25)	(36.68)	(1.88)		(0.01)	(3.23)	(15.94)	(1.58)
SYM-5	-0.15	0.01	60.62	-3.23	24.73	0.69	0.004	26.48	25.90	9.11	0.76	0.01	17.89	8.14	10.02
		(0.004)	(20.53)	(29.63)	(4.19)		(0.002)	(11.38)	(22.37)	(2.59)		(0.003)	(4.21)	(9.58)	(1.94)
SYM-10	-0.03	0.01	58.04	14.49	25.84	0.47	0.01	30.84	25.86	10.10	0.53	0.01	24.21	11.80	11.12
		(0.005)	(15.19)	(43.60)	(3.29)		(0.002)	(7.72)	(19.74)	(3.46)		(0.004)	(5.89)	(6.60)	(1.72)
ASYM-5	0.27	0.01	49.28	8.66	26.67	0.84	0.01	18.89	27.66	9.78	0.79	0.01	16.21	-1.39	8.42
		(0.004)	(14.04)	(32.25)	(6.80)		(0.004)	(3.01)	(19.06)	(3.31)		(0.004)	(2.84)	(7.09)	(2.58)
ASYM-10	0.25	0.01	48.86	15.18	25.28	0.81	0.01	24.85	44.33	10.48	0.73	0.02	19.71	12.41	9.73
		(0.004)	(7.94)	(33.59)	(5.78)		(0.004)	(4.05)	(18.88)	(2.02)		(0.01)	(4.34)	(6.24)	(1.58)

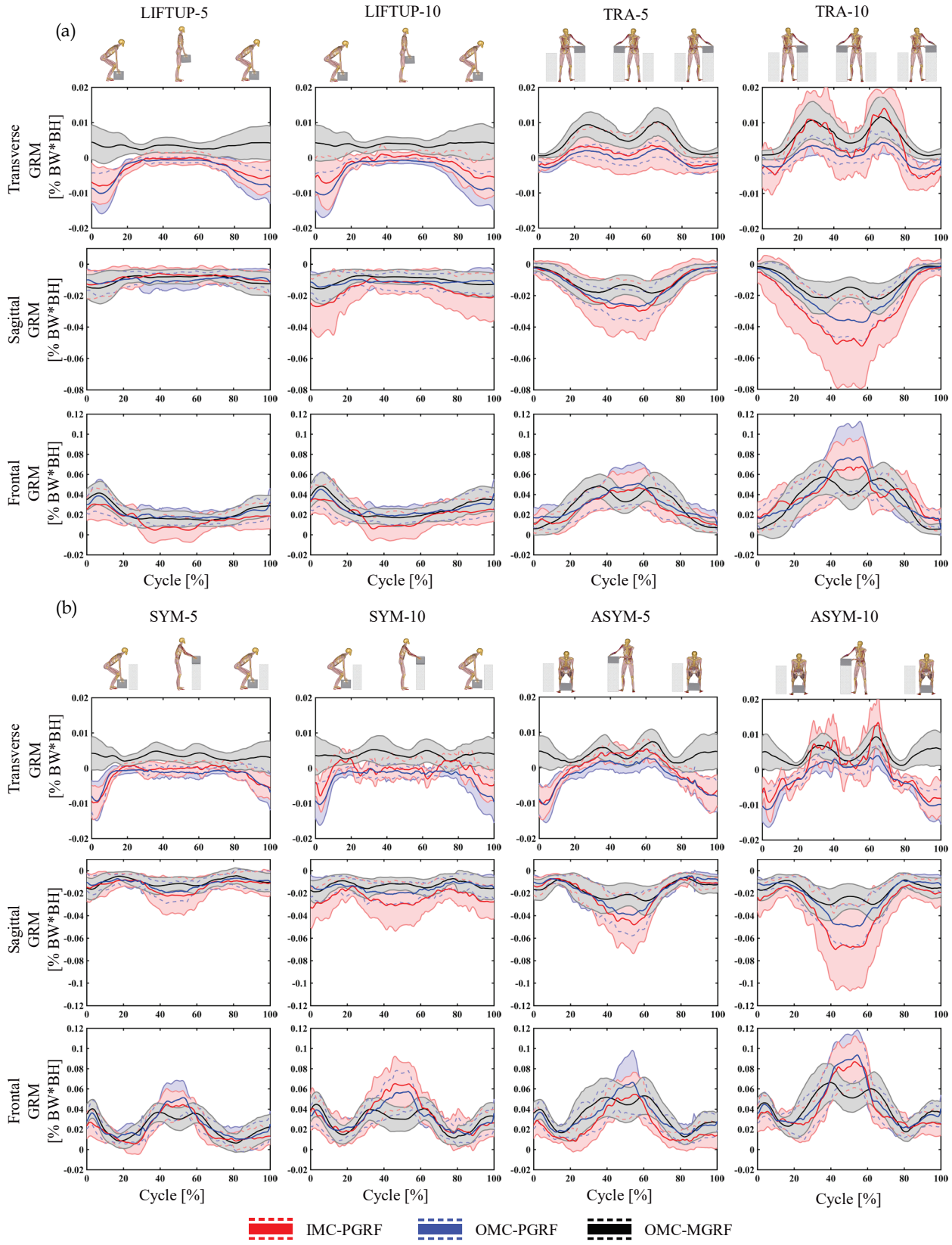

Fig. 4: GRM estimates for the right foot (SD around mean) of the IMC-PGRF (red-shaded area around red line), OMC-PGRF (blue-shaded area around blue line), and OMC-MGRF (black-shaded area around black line) models, illustrating the transverse GRM, sagittal GR6M, and frontal GRM from (a) LIFTUP-5, LIFTUP-10, TRA-5, TRA-10, and (b) SYM-5, SYM-10, ASYM-5, and ASYM-10.

3.3 Estimated joint reaction forces

Overall, strong to excellent correlations were observed in axial compression forces and anteroposterior shear forces between IMC-PGRF and OMC-MGRF (see Table 5) for all lifting tasks (ρ ranging from 0.77 to 0.99). However, higher correlations were found between OMC-PGRF and OMC-MGRF (see Table 6) in both axial and anteroposterior directions (ρ 0.99). Mediolateral shear forces were found to have weak to moderate correlations (ρ ranging from 0.05 to 0.47) between IMC-PGRF and OMC-MGRF opposed to OMC-PGRF which had excellent correlations to OMC-MGRF (ρ 0.99). Also, RMSE values were noticeably higher in axial compression forces for IMC-PGRF (RMSE ranging from IMC-PGRF: 47.31 to 87.13 % versus OMC-PGRF: 0.37 to 14.86 %). Similar tendency in RMSE values were observed for mediolateral and anteroposterior shear forces, and in rRMSE values for all directions (rRMSE ranging from IMC-PGRF: 15.26 to 75.43 % versus OMC-PGRF: 0.15 to 6.41 %). Magnitude differences were specifically large for IMC-PGRF in mediolateral shear forces during tasks involving lifting or transferring of the 10 kg box (M ranging from IMC-PGRF: 43.29 to 148.61 % versus OMC-PGRF: -6.34 to 0.98 %). In general, all directions exhibited large inter-subject magnitude variability for IMC-PGRF. IMC-PGRF phase differences values, however, performed with high accuracy in axial compression forces and anteroposterior shear forces (P ranging from IMC-PGRF: 1.36 to 5.00 % versus OMC-PGRF 0.03 to 0.79 %), whereas mediolateral shear forces showed larger phase lag for IMC-PGRF (P ranging from IMC-PGRF: 18.01 to 23.04 % versus OMC-PGRF 0.37 to 02.05 %).

Table 5: IMC-PGRF-based JRFs versus OMC-MGRF for the eight lifting scenarios. ρ = Pearson's correlation coefficient, RMSE = root mean square error (%BW), rRMSE = relative root mean square error (%), M = curve magnitude difference (%), and P = phase difference (%). Results are for axial compression force, mediolateral shear force, and anteroposterior shear force. All results are presented as mean (± SD).

Activity	Axial compression force					Mediolateral shear force					Anteroposterior shear force				
	ρ	RMSE	rRMSE	M	P	ρ	RMSE	rRMSE	M	P	ρ	RMSE	rRMSE	M	P
LIFTUP-5	0.99	53.41	24.95	8.73	3.27	0.26	1.85	75.43	2.60	23.04	0.99	12.65	32.03	-29.88	3.76
		(45.42)	(18.11)	(15.80)	(1.81)		(0.80)	(47.73)	(48.50)	(7.29)		(6.00)	(16.89)	(11.71)	(2.23)
LIFTUP-10	0.98	59.80	17.90	9.34	2.73	0.25	3.03	53.17	123.01	20.65	0.97	12.75	23.47	-22.48	3.99
		(52.30)	(6.82)	(16.09)	(1.02)		(1.68)	(35.07)	(120.1)	(6.13)		(6.00)	(12.43)	(12.73)	(1.56)
TRA-5	0.86	47.76	72.43	13.38	1.36	0.21	2.98	37.44	34.38	22.37	0.91	7.04	46.02	8.61	2.69
		(41.78)	(41.75)	(18.90)	(0.55)		(1.15)	(10.49)	(61.70)	(5.43)		(4.57)	(29.13)	(31.55)	(0.95)
TRA-10	0.77	87.13	56.43	26.29	2.16	0.21	5.79	38.26	147.33	19.53	0.78	11.73	33.13	24.46	3.22
		(59.36)	(32.06)	(17.00)	(0.71)		(1.84)	(15.51)	(145.6)	(7.63)		(7.12)	(17.86)	(20.87)	(0.81)
SYM-5	0.93	58.55	28.15	13.80	2.62	0.34	1.71	61.25	1.75	22.64	0.91	12.52	31.85	-25.66	4.28
		(40.85)	(13.80)	(14.61)	(1.12)		(0.75)	(54.95)	(55.36)	(4.97)		(7.41)	(21.76)	(11.20)	(2.82)
SYM-10	0.91	71.66	23.62	14.38	2.44	0.05	3.68	72.90	43.29	21.91	0.82	11.45	21.11	-9.70	5.00
		(49.72)	(6.00)	(14.39)	(0.68)		(1.01)	(41.44)	(94.05)	(5.58)		(5.18)	(9.82)	(12.77)	(1.66)
ASYM-5	0.99	47.31	19.69	10.24	1.88	0.47	2.89	39.41	16.62	18.01	0.98	9.58	20.68	-19.46	2.75
		(43.42)	(12.51)	(15.62)	(0.58)		(1.28)	(13.49)	(59.66)	(6.33)		(6.33)	(11.00)	(9.61)	(0.84)
ASYM-10	0.91	78.31	26.43	18.21	2.90	0.34	6.39	45.49	148.61	19.13	0.89	9.50	15.26	-5.09	4.50
		(44.13)	(7.39)	(10.28)	(0.55)		(2.28)	(16.43)	(148.7)	(6.21)		(5.23)	(3.79)	(9.79)	(1.16)

Table 6: OMC-PGRF-based JRFs versus OMC-MGRF for the eight lifting scenarios. ρ = Pearson's correlation coefficient, RMSE = root mean square error (%BW), rRMSE = relative root mean square error (%), M = curve magnitude difference (%), and P = phase difference (%). Results are for axial compression force, mediolateral shear force, and anteroposterior shear force. All results are presented as mean (± SD).

Activity	Axial compression force					Mediolateral shear force					Anteroposterior shear force				
	ρ	RMSE	rRMSE	M	P	ρ	RMSE	rRMSE	M	P	ρ	RMSE	rRMSE	M	P
LIFTUP-5	0.99	0.37	0.15	-0.09	0.03	0.99	0.02	0.85	0.98	0.57	0.99	0.09	0.17	-0.20	0.04
		(0.10)	(0.04)	(0.05)	(0.01)		(0.02)	(0.68)	(1.19)	(0.58)		(0.08)	(0.15)	(0.14)	(0.02)
LIFTUP-10	0.99	3.91	1.48	-1.22	0.19	0.99	0.05	1.81	-0.10	1.35	0.99	0.86	1.82	-2.02	0.39
		(12.46)	(4.80)	(4.00)	(0.61)		(0.09)	(3.30)	(5.09)	(2.78)		(2.66)	(5.90)	(6.56)	(1.27)
TRA-5	0.99	0.57	0.74	-0.20	0.03	0.99	0.03	0.51	-0.49	0.37	0.99	0.13	0.70	-0.35	0.06
		(0.30)	(0.34)	(0.11)	(0.02)		(0.02)	(0.31)	(0.67)	(0.27)		(0.14)	(0.57)	(0.34)	(0.03)
TRA-10	0.99	5.46	6.41	-1.75	0.18	0.99	0.08	1.55	-1.99	0.98	0.99	0.97	5.50	-2.36	0.24
		(15.27)	(19.10)	(5.06)	(0.45)		(0.11)	(2.63)	(4.66)	(1.59)		(2.62)	(15.95)	(6.65)	(0.55)
SYM-5	0.99	0.88	0.41	-0.19	0.06	0.99	0.03	0.68	-0.04	0.69	0.99	0.14	0.29	-0.21	0.06
		(0.60)	(0.31)	(0.07)	(0.06)		(0.02)	(0.42)	(0.70)	(0.52)		(0.10)	(0.21)	(0.12)	(0.07)
SYM-10	0.99	5.33	2.52	-1.31	0.34	0.99	0.15	2.95	-4.16	1.79	0.99	0.92	2.47	-1.71	0.42
		(12.25)	(6.31)	(3.50)	(0.78)		(0.20)	(4.85)	(8.62)	(2.13)		(2.69)	(7.69)	(5.37)	(1.28)
ASYM-5	0.99	0.51	0.21	-0.15	0.03	0.99	0.04	0.51	-0.31	0.42	0.99	0.08	0.16	-0.17	0.03
		(0.13)	(0.08)	(0.04)	(0.01)		(0.02)	(0.24)	(0.57)	(0.30)		(0.03)	(0.07)	(0.06)	(0.01)
ASYM-10	0.99	14.86	5.35	-3.47	0.50	0.99	0.25	3.96	-6.34	2.05	0.99	3.04	5.84	-5.24	0.79
		(27.12)	(9.52)	(6.20)	(0.86)		(0.40)	(6.64)	(12.98)	(3.12)		(5.68)	(10.71)	(9.60)	(1.44)

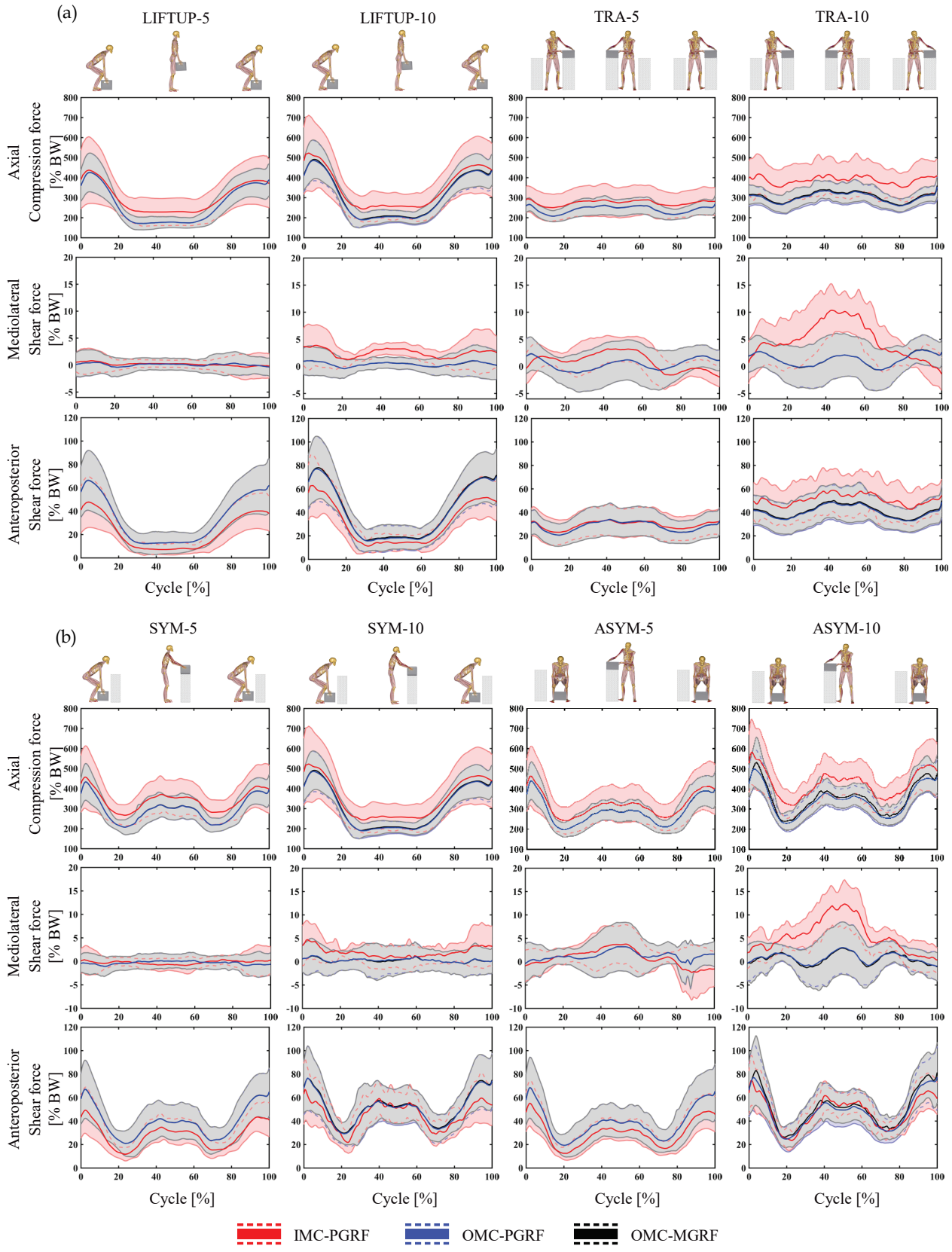

Fig. 5: JRF estimates (SD around mean) of the IMC-PGRF (red-shaded area around red line), OMC-PGRF (blue-shaded area around blue line), and OMC-MGRF (black-shaded area around black line) models, illustrating the axial compression force, mediolateral shear force, and anteroposterior shear force from (a) LIFTUP-5, LIFTUP-10, TRA-5, TRA-10, and (b) SYM-5, SYM-10, ASYM-5, and ASYM-10.

4. Discussion

The accuracy of three IDA musculoskeletal models have been investigated to estimate the internal spinal loading during common MMH tasks. The experimental model with OMC-MGRF was considered the golden standard because a previous study (Bassani et al., 2017) has shown good agreement with in vivo measured intradiscal L4-L5 spinal pressure (Wilke et al., 2001). A novel IMC-PGRF model was developed to compare predicted GRF&Ms and internal L4-L5 JRFs with the OMC-MGRF model. Estimated vertical GRF, sagittal and frontal GRM, axial compression forces, and anteroposterior shear forces agreed best for IMC-PGRF compared with OMC-MGRF. Finally, we performed a similar comparison to evaluate predicted GRF&Ms and JRFs with the OMC-PGRF model. The differences are discussed in the following.

Experimental measurements of GRF&Ms was collected during all lifting trials allowing direct comparison similar to other studies (Faber et al., 2016; Fluit et al., 2014; Karatsidis et al., 2018; Peng et al., 2017; Skals et al., 2017a, 2017b). The present study found best agreement for predicted vertical GRFs for IMC-PGRF compared with OMC-MGRF considering Pearson's correlation coefficients, rRMSE and magnitude and phase difference, whereas mediolateral and anteroposterior agreed less. Particularly, transferring and asymmetrical tasks showed excellent correlations in vertical GRFs similar to OMC-PGRF versus OMC-MGRF. Although, increasing the box weight from 5 to 10 kg increased the magnitude error, RMSE, and rRMSE systematically for IMC-PGRF models (Table 1). This may be considered an important factor if heavier weights introduce greater errors (see worksheets 3.0 *method*).

For the symmetric lifting tasks, the vertical GRF magnitude appeared to be more constant throughout the lifting cycle with peaks in the beginning and end of the cycle (see Fig. 3). In contrast, transferring and asymmetric tasks showed a more varying magnitude across the time-series with peak vertical GRFs around the mid-cycle. This difference was introduced by only presenting GRFs for the right foot. Thus, a considerably shift in center of pressure and force magnitude were introduced for transferring and asymmetric lifting tasks because they included movement out of the sagittal plane whereas GRFs were evenly distributed between both feet during symmetric lifting tasks. This demonstrate good accuracy in the contact element actuation for both the IMC-PGRF and OMC-PGRF models.

In the present study, novel movements were investigated with IMC and GRF&Ms prediction, and to our knowledge only Faber et al. (2016) estimated GRF for a trunk bending tasks using IMC. Other studies primarily predicted GRF&Ms for activities of daily living including walking, running squatting, stair walking, and loaded shoulder abduction using OMC or other measuring systems such as Microsoft Kinect (Faber et al., 2016; Fluit et al., 2014; Karatsidis et al., 2018; Peng et al., 2017; Skals et al., 2017a, 2017b). Faber et al. (2016) showed similar results to the present study with best agreement in vertical GRFs. This agrees with the above-mentioned literature generally showing most accurate estimation for vertical GRFs. In addition, IMC-PGRF showed higher correlations and slightly lower phase error in vertical GRFs for LIFTUP-5 (ρ: 0.87 and P: 2.55 %) as opposed to a deep squat movement estimated with OMC-PGRF (ρ: 0.62 and P: 2.7 %) presented in Fluit et al. (2014).

Importantly, considerable differences exist between vertical GRFs for both IMC-PGRF and OMC-PGRF versus OMC-MGRF at approximately 50 % of the lifting cycle for SYM-5/10, ASYM-5/10, and TRA-5/10 conditions (see Fig. 3). This was caused by the support of the tables in the period where the box was in contact (see Fig. 1 Mid-cycle). Potentially, contact elements could be attached to the box in AMS. However, this would require modelling of the support surfaces in the model environment and would be affected by IMC spatial drift (Filippeschi et al., 2017). Therefore, this was neglected and noted as a limitation. Another solution would be to attach force transducers to the handles of the box (Dennis and Barrett, 2002).

The errors of GRMs for the IMC-PGRF model were generally higher compared to other studies investigating other movements (Fluit et al., 2014; Karatsidis et al., 2018; Peng et al., 2017; Ren et al., 2008; Skals et al., 2017a, 2017b). Differences between the results of these studies can partly be explained by differences in movement complexity (Godwin et al., 2009), influence of spatial drift of the IMC system (Filippeschi et al., 2017), and the relatively low magnitude which increased the influence of noise.

Magnitude error values showed large differences for both IMC-PGRF and OMC-PGRF models for GRMs in all directions. However, a distinct disadvantage to Sprague and Geers magnitude algorithm is that positive and negative differences may cancel each other out (Schwer, 2007). Standard deviations (SDs) were excessively high for GRMs, and as illustrated in Fig. 4, SD curves of both IMC-PGRF, OMC-PGRF, and OMC-MGRF is both negative and positive arranged for most lifting tasks. This shows that the magnitude error algorithm has limitations when SDs are excessively high. This observation also reveals that the OMC-PGRF model suffer from errors of similar size as IMC-PGRF when predicting moments. SDs were considerably smaller in phase differences, displaying less influence of phase difference between models.

Accurate estimation of JRFs between the vertebral bodies

using the IMC-PGRF musculoskeletal model as an analysis tool may revolutionize ergonomic analysis of MMH in the field. Fig. 5 visually presents the JRF time-series curves for the different lifting and transferring tasks. Axial compression force and anteroposterior shear force for IMC-PGRF showed higher correlations to OMC-MGRF (ρ ranging from 0.77 to 0.99) than mediolateral shear force (Table 5). A similar tendency were found by Karatsidis et al. (2018) showing higher correlations for compression forces for the ankle, knee, and hip joint (ρ ranging from 0.83 to 0.93). Also, minimal phase differences were observed for the present study suggesting a minimal difference in time-shift between IMC-PGRF and OMC-PGRF. Magnitudes for IMC-PGRF were overestimated for axial compression force and underestimated for anteroposterior shear force. Specifically, during transferring and asymmetric lifting, the magnitude errors were larger when the weight of the box increased, similar to the errors found in vertical GRFs (Table 1). Axial compression force error was noticeable smaller for both magnitude and phase error for OMC-PGRF compared with OMC-MGRF. Differences between IMC-PGRF and OMC-PGRF may be caused by segment lengths, kinematics, and due to different boundary conditions concerning the interaction with the box (see worksheet 3.3.4 *Modelling hand box interaction*). Similar to Koblauch et al. (2015), the peak axial compression force was found when the subjects were carrying the box at the longest distance from the body (see Fig. 5 and Appendix 1 - L4-L5 in Koblauch et al. (2015)). Although the geometry of the box, the participant characteristics, and the specific movements differed between the present study and Koblauch et al. (2015), it seems that the magnitude of JRFs was reasonable with peak L4-L5 axial compression force of ~3450 N during squat lifting of a 10 kg suitcase in Koblauch et al. (2015) and ~3850 N during symmetric lifting of a 10 kg box in the present study measured with IMC-PGRF.

The present work was associated with several limitations. Although the OMC-MGRF was assumed the gold standard it is well-known that magnitudes of estimated spinal loadings are less accurate during large lateral bending movements (Bassani et al., 2017) and sensitive to model complexities such as spine rhythm, intra-abdominal pressure, joint stiffness, musculature, and ligaments (Arshad et al., 2016; Galibarov et al., 2011; Han et al., 2012). Therefore, also estimates of spinal loading using the gold standard method has uncertainties. Furthermore, measurements of human movements are prone to STA with most research showing the largest influence of STA on movement in the frontal and transverse planes (Leardini et al., 2005). However, the present study investigated movements at a slow pace minimizing large STA opposed to e.g. running where large impacts are more prominent. Furthermore, incorrect determination of anatomical joint coordinate systems significantly influences the segment kinematics (Della Croce et al., 1999) from which predicted GRF&Ms are found (Fluit et al., 2014). Also, OMC was scaled according to attachment of reflective markers while IMC models was scaled of manually measured segment dimensions, which might have introduced differences in segment lengths. The accuracy of box tracking may also be improved with IMUs attached to the box, and with force transducers in the handles similar to Dennis and Barrett (2002). Moreover, a sensitivity analysis could have been performed on the muscle recruitment criteria to investigate the influence on L4-L5 load magnitude (Fluit et al., 2014). Lastly, a risk of not fully extended joint angles during the calibration process, might have influenced the estimated joint angles with IMC (Cutti et al., 2010; Roetenberg et al., 2013).

Future studies should investigate the accuracy of estimated L4-L5 loading in patient populations such as patients suffering from chronic low back pain because they may not recruit their muscles optimally (Bank et al., 2013; Rasmussen et al., 2001). The method shows potential for measuring spinal loading outside the laboratory. Future work should validate and adapt the system to MMH work environments.

In summary, the accuracy of predicted GRF&Ms as well as estimated L4-L5 JRFs were investigated using an inverse dynamic musculoskeletal modelling approach based on IMC data. The analysis showed that IMC-PGRF can be used to estimate musculoskeletal loading during standard MMH task such as symmetric, asymmetric, and transferring lifting tasks with reasonable results compared with OMC-MGRF and OMC-PGRF. Specifically, vertical GRFs, axial compression forces, and anteroposterior shear forces showed high accuracy for all lifting tasks. The inaccuracies associated with IMC-PGRF have been investigated and can be used as considerations in future studies. The method can be used in the field to estimate musculoskeletal loading during simple MMH tasks where the geometry and inertia of external loads can be estimated and used as input to the model.

5. Conflict of interest

None of the authors have any financial or personal conflict of interest regarding this study.

6. References

Adams, M.A., Hutton, W.C., 1983. The mechanics of prolapsed intervertebral disc. Int. Orthop. 6, 249–253.

Andersen, M.S., 2009. Kinematically over-determinate biomechanical systems.

Andersen, M.S., Damsgaard, M., MacWilliams, B., Rasmussen, J., 2010. A computationally efficient optimisation-based method for parameter identification of kinematically determinate and over-determinate biomechanical systems. Comput. Methods Biomech. Biomed. Engin. 13, 171–183.

Andersen, M.S., Damsgaard, M., Rasmussen, J., 2009. Kinematic analysis of over-determinate biomechanical systems. Comput. Methods Biomech. Biomed. Engin. 12, 371–384.

Anderson, C.K., Chaffin, D.B., Herrin, G.D., Matthews, L.S., 1985. A biomechanical model of the lumbosacral joint during lifting activities. J. Biomech. 18, 571–584.

Andersson, G.B.J., 1999. Epidemiological features of chronic low-back pain. Lancet 354, 581–585.

Arshad, R., Zander, T., Dreischarf, M., Schmidt, H., 2016. Influence of lumbar spine rhythms and intra-abdominal pressure on spinal loads and trunk muscle forces during upper body inclination. Med. Eng. Phys. 38, 333–338.

Bank, P.J.M., Peper, C.E., Marinus, J., Beek, P.J., Van Hilten, J.J., 2013. Motor consequences of experimentally induced limb pain: A systematic review. Eur. J. Pain 17, 145–157.

Barrett, R.S., Besier, T.F., Lloyd, D.G., 2007. Individual muscle contributions to the swing phase of gait: An EMG-based forward dynamics modelling approach. Simul. Model. Pract. Theory 15, 1146–1155.

Bassani, T., Stucovitz, E., Qian, Z., Briguglio, M., Galbusera, F., 2017. Validation of the AnyBody full body musculoskeletal model in computing lumbar spine loads at L4L5 level. J. Biomech. 58, 89–96.

Brinckmann, P., Biggemann, M., Hilweg, D., 1989. Prediction of the compressive strength of human lumbar vertebrae. Spine. 14, 606–610.

Brinckmann, P., Frobin, W., Biggemann, M., Hilweg, D., Seidel, S., Burton, K., Tillotson, M., Sandover, J., Atha, J., Quinnell, R., 1998. Quantification of overload injuries to thoracolumbar vertebrae and discs in persons exposed to heavy physical exertions or vibration at the work-place. The shape of vertebrae and intervertebral discs - study of a young, healthy population and a middle-age. Clin. Biomech. 13, 1–36.

Carbone, V., Fluit, R., Pellikaan, P., van der Krogt, M.M., Janssen, D., Damsgaard, M., Vigneron, L., Feilkas, T., Koopman, H.F.J.M., Verdonschot, N., 2015. TLEM 2.0 - A comprehensive musculoskeletal geometry dataset for subject-specific modeling of lower extremity. J. Biomech. 48, 734–741.

Cole, M.H., Grimshaw, P.N., 2003. Low back pain and lifting: a review of epidemiology and aetiology. Work 21, 173–184.

Cutti, A.G., Ferrari, A., Garofalo, P., Raggi, M., Cappello, A., Ferrari, A., 2010. "Outwalk": A protocol for clinical gait analysis based on inertial and magnetic sensors. Med. Biol. Eng. Comput. 48, 17–25.

Damsgaard, M., Rasmussen, J., Christensen, S.T., Surma, E., de Zee, M., 2006. Analysis of musculoskeletal systems in the AnyBody Modeling System. Simul. Model. Pract. Theory 14, 1100–1111.

de Zee, M., Hansen, L., Wong, C., Rasmussen, J., Simonsen, E.B., 2007. A generic detailed rigid-body lumbar spine model. J. Biomech. 40, 1219–1227.

Della Croce, U., Cappozzo, A., Kerrigan, D.C., 1999. Pelvis and lower limb anatomical landmark calibration precision and its propagation to bone geometry and joint angles. Med. Biol. Eng. Comput. 37, 155–161.

Dempsey, P.G., 1998. A critical review of biomechanical, epidemiological, physiological and psychophysical criteria for designing manual materials handling tasks. Ergonomics 41, 73–88.

Dennis, G.J., Barrett, R.S., 2002. Spinal loads during individual and team lifting. Ergonomics 45, 671–681.

Dreischarf, M., Shirazi-Adl, A., Arjmand, N., Rohlmann, A., Schmidt, H., 2016. Estimation of loads on human lumbar spine: A review of in vivo and computational model studies. J. Biomech. 49, 833–845.

Faber, G.S., Chang, C.C., Kingma, I., Dennerlein, J.T., van Dieën, J.H., 2016. Estimating 3D L5/S1 moments and ground reaction forces during trunk bending using a full-body ambulatory inertial motion capture system. J. Biomech. 49, 904–912.

Faber, G.S., Kingma, I., Delleman, N., van Dieën, J., 2008. Effect of ship motion on spinal loading during manual lifting. Ergonomics 51, 1426–1440.

Filippeschi, A., Schmitz, N., Miezal, M., Bleser, G., Ruffaldi, E., Stricker, D., 2017. Survey of Motion Tracking Methods Based on Inertial Sensors: A Focus on Upper Limb Human Motion. Sensors 17, 1257.

Fluit, R., Andersen, M.S., Kolk, S., Verdonschot, N., Koopman, H.F.J.M.J.M., 2014. Prediction of ground reaction forces and moments during various activities of daily living. J. Biomech. 47, 2321–2329.

Frankenfield, D.C., Rowe, W.A., Cooney, R.N., Smith, J.S., Becker, D., 2001. Limits of body mass index to detect obesity and predict body composition. Nutrition 17, 26–30.

Galibarov, P.E., Dendorfer, S., Rasmussen, J., 2011. Two Computational Models of the Lumbar Spine: Comparison and Validation. ORS Annu Meet 2011.

Godwin, A., Agnew, M., Stevenson, J., 2009. Accuracy of Inertial Motion Sensors in Static, Quasistatic, and Complex Dynamic Motion. J. Biomech. Eng. 131, 114501.

Han, K.S., Zander, T., Taylor, W.R., Rohlmann, A., 2012. An enhanced and validated generic thoraco-lumbar spine model for prediction of muscle forces. Med. Eng. Phys. 34, 709–716.

Hansen, L., De Zee, M., Rasmussen, J., Andersen, T.B., Wong, C., Simonsen, E.B., 2006. Anatomy and biomechanics of the back muscles in the lumbar spine with reference to biomechanical modeling. Spine. 31, 1888–1899.

Karatsidis, A., Bellusci, G., Schepers, H., de Zee, M., Andersen, M., Veltink, P., 2016. Estimation of Ground Reaction Forces and Moments During Gait Using Only Inertial Motion Capture. Sensors 17, 75.

Karatsidis, A., Jung, M., Schepers, H.M., Bellusci, G., de Zee, M., Veltink, P.H., Andersen, M.S., 2018. Predicting kinetics using musculoskeletal modeling and inertial motion capture. Arxiv.org.

Kim, S., Nussbaum, M.A., 2013. Performance evaluation of a wearable inertial motion capture system for capturing physical exposures during manual material handling tasks. Ergonomics 56, 314–326.

Koblauch, H., 2015. Low back load in airport baggage handlers. Grad. Sch. Fac. Heal. Med. Sci. Univ. Copenhagen. University of Copenhagen.

Koning, B.H.W., van der Krogt, M.M., Baten, C.T.M., Koopman, B.F.J.M., 2015. Driving a musculoskeletal model with inertial and magnetic measurement units. Comput. Methods Biomech. Biomed. Engin. 18, 1003–1013.

Leardini, A., Chiari, A., Della Croce, U., Cappozzo, A., 2005. Human movement analysis using stereophotogrammetry Part 3. Soft tissue artifact assessment and compensation. Gait Posture 21, 212–225.

Moisio, K.C., Sumner, D.R., Shott, S., Hurwitz, D.E., 2003. Normalization of joint moments during gait: A comparison of two techniques. J. Biomech. 36, 599–603.

Pandy, M.G., Andriacchi, T.P., 2010. Muscle and joint function in human locomotion., Annual review of biomedical engineering.

Peng, Y., Zhang, Z., Gao, Y., Chen, Z., Xin, H., Zhang, Q., Fan, X., Jin, Z., 2017. Concurrent prediction of ground reaction forces and moments and tibiofemoral contact forces during walking using musculoskeletal modelling. Med. Eng. Phys. 0, 1–10.

Rajaee, M.A., Arjmand, N., Shirazi-Adl, A., Plamondon, A., Schmidt, H., 2015. Comparative evaluation of six quantitative lifting tools to estimate spine loads during static activities. Appl. Ergon. 48, 22–32.

Rasmussen, J., Damsgaard, M., Voigt, M., 2001. Muscle recruitment by the min/max criterion - A comparative numerical study. J. Biomech. 34, 409–415.

Rasmussen, J., de Zee, M., Carbes, S., 2009. Validation of a biomechanical model fo the lumbar spine, in: Congress XXII of the International Society of Biomechanics.

Rasmussen, J., De Zee, M., Damsgaard, M., Tørholm Christensen, S., Marek, C., Siebertz, K., 2005. A general method for scaling musculo-skeletal models. 2005 Int. Symp. Comput. Simul. Biomech. 3.

Ren, L., Jones, R.K., Howard, D., 2008. Whole body inverse dynamics over a complete gait cycle based only on measured kinematics. J. Biomech. 41, 2750–2759.

Roetenberg, D., Luinge, H.J., Slycke, P., 2013. Xsens MVN : Full 6DOF Human Motion Tracking Using Miniature Inertial Sensors. Enschede, The Netherlands.

Schwer, L.E., 2007. Validation metrics for response histories: Perspectives and case studies. Eng. Comput. 23, 295–309.

Skals, S., Jung, M.K., Damsgaard, M., Andersen, M.S., 2017a. Prediction of ground reaction forces and moments during sports-related movements. Multibody Syst. Dyn. 39, 175–195.

Skals, S., Rasmussen, K.P., Bendtsen, K.M., Yang, J., Andersen, M.S., 2017b. A musculoskeletal model driven by dual Microsoft Kinect Sensor data. Multibody Syst. Dyn. 41, 297–316.

Sprague, M.A., Geers, T.L., 2003. Spectral elements and field separation for an acoustic fluid subject to cavitation. J. Comput. Phys. 184, 149–162.

Taylor, R., 1990. Interpretation of the Correlation Coefficient: A Basic Review. J. Diagnostic Med. Sonogr. 6, 35–39.

Van der Helm, F.C.T., Veeger, H.E.J., Pronk, G.M., Van der Woude, L.H.V., Rozendal, R.H., 1992. Geometry parameters for musculoskeletal modelling of the shoulder system. J. Biomech. 25, 129–144.

van Dieën, J.H., Faber, G.S., Loos, R.C.C., Kuijer, P.P.F.M., Kingma, I., van der Molen, H.F., Frings-Dresen, M.H.W., 2010. Validity of estimates of spinal compression forces obtained from worksite measurements. Ergonomics 53, 792–800.

Van Dieën, J.H., Weinans, H., Toussaint, H.M., 1999. Fractures of the lumbar vertebral endplate in the etiology of low back pain: A hypothesis on the causative role of spinal compression in aspecific low back pain. Med. Hypotheses 53, 246–252.

Veeger, H.E.J., Van Der Helm, F.C.T., Van Der Woude, L.H.V., Pronk, G.M., Rozendal, R.H., 1991. Inertia and Muscle-Contraction Parameters for Musculoskeletal Modeling of the Shoulder Mechanism. J. Biomech. 24, 615-.

Veeger, H.E.J., Yu, B., An, K.N., Rozendal, R.H., 1997. Parameters for modeling the upper extremity. J. Biomech. 30, 647–652.

Veltink, P.H., Liedtke, C., Droog, E., Van Der Kooij, H., 2005. Ambulatory measurement of ground reaction forces. IEEE Trans. Neural Syst. Rehabil. Eng. 13, 423–427.

Waters, T., Yeung, S., Genaidy, A., Callaghan, J., Barriera-Viruet, H., Deddens, J., 2006. Cumulative spinal loading exposure methods for manual material handling tasks. Part 1: Is cumulative spinal loading associated with lower back disorders? Theor. Issues Ergon. Sci. 7, 113–130.

Wilke, H.-J., Neef, P., Hinz, B., Seidel, H., Claes, L., 2001. Intradiscal pressure together with anthropometric data – a data set for the validation of models. Clin. Biomech. 16, Supple, S111--S126.

Winter, D.A., 2009. Biomechanics and Motor Control of Human Movement, 4th ed. ed. Hoboken, N.J. : John Wiley.

Wong, K.W.N., Luk, K.D.K., Leong, J.C.Y., Wong, S.F., Wong, K.K.Y., 2006. Continuous Dynamic Spinal Motion Analysis. Spine (Phila. Pa. 1976). 31, 414–419.

Xsens Technologies, 2017. Quick setup: getting started with xsens mvn. Enschede, The Netherlands.

Appendix 1

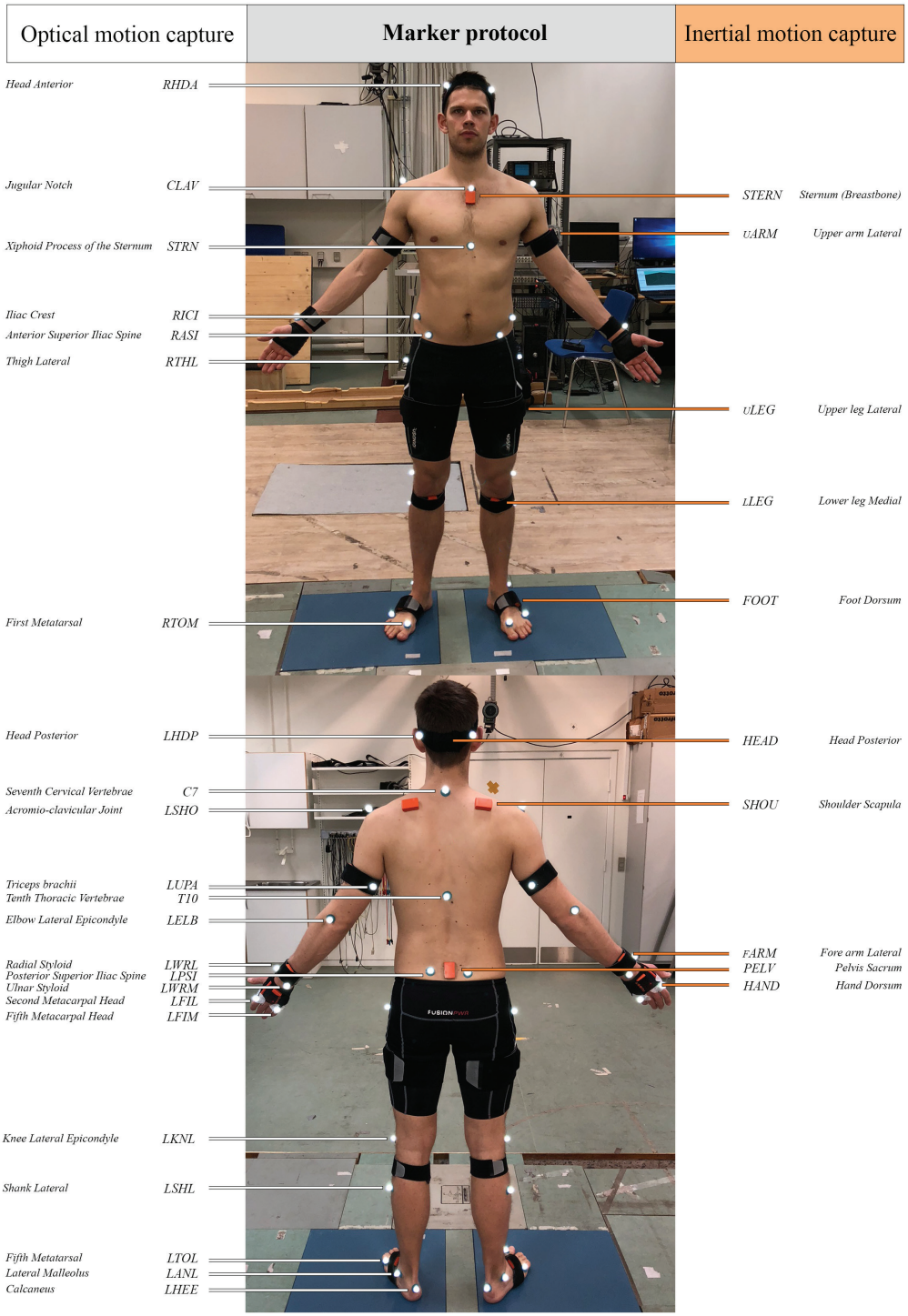

Appendix 1: Motion capture protocol indicating the placement of the 42 retroreflective markers on the human body segments (left on the figure) and the 17 IMUs (right on the figure). All retroreflective markers apart from T10, C7, STRN, and CLAV and all IMUs apart from PELV, STERN, and HEAD, are mirrored on left and right side.